

A scalable control system for a superconducting adiabatic quantum optimization processor

M. W. Johnson[†], P. Bunyk[‡], F. Maibaum[‡], E. Tolkacheva[†], A. J. Berkley[†], E. M. Chapple[†], R. Harris[†], J. Johansson[†], T. Lanting[†], I. Perminov[†], E. Ladizinsky[†], T. Oh[†], G. Rose[†]

Abstract— We have designed, fabricated and operated a scalable system for applying independently programmable time-independent, and limited time-dependent flux biases to control superconducting devices in an integrated circuit. Here we report on the operation of a system designed to supply 64 flux biases to devices in a circuit designed to be a unit cell for a superconducting adiabatic quantum optimization system. The system requires six digital address lines, two power lines, and a handful of global analog lines.

I. INTRODUCTION

Several proposals for how one might implement a quantum computer now exist. One of these is based on enabling adiabatic quantum optimization algorithms in networks of superconducting flux qubits connected via tunable coupling devices [1]. Flux qubits can be manipulated by applying magnetic flux via currents along inductively coupled control lines. This can be accomplished with one analog control line per device driven by room temperature current sources and routed, through appropriate filtering, down to the target device on chip.

Beyond the scale of a few dozens of such qubits the *one analog line per device* approach becomes impractical. Hundreds of qubits could require thousands of wires, each subject to filtering, cross-talk, and thermal requirements so as to minimize disturbance of the thermal and electromagnetic environment of the targeted qubits, which are operated at milliKelvin temperatures. We require an approach that does not use so many wires.

One advantage of using superconductor based qubits is the existence of a compatible classical digital and mixed signal electronics technology based on the manipulation of single-flux-quanta (SFQ) [2]. The ability to manufacture classical control circuitry [3] on the same chip, with the same fabrication technology as is used in construction of the qubits, addresses many of the thermal and electromagnetic compatibility requirements faced in integrating control circuitry with such a processor.

We present here a description of a functioning system of on-chip Programmable Control Circuitry (PCC) designed to manipulate the parameters and state of superconducting flux qubits and tunable couplers, in such a way as to overcome the scalability limitations of the *one analog line per device* paradigm. This system comprises three key parts.

[†] D-Wave Systems Inc., 100-4401 Still Creek Dr., Burnaby, BC V5C 6G9 Canada (mwjohnson@dwavesys.com).

[‡] Physikalisches Technische Bundesanstalt, Bundesallee 100, 38116 Braunschweig, Germany

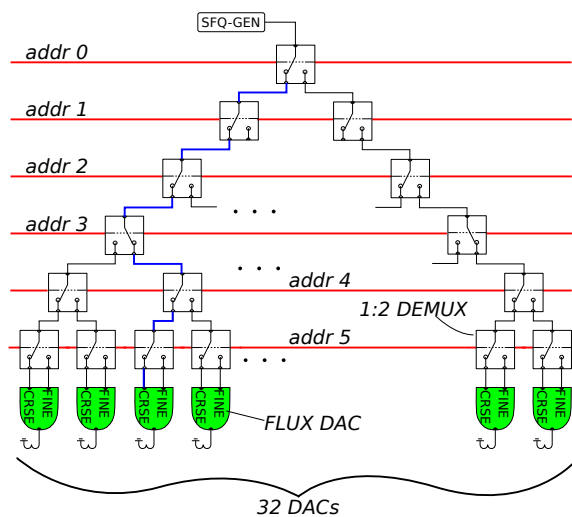


Fig. 1. A 1:32 demultiplexer tree terminating in two-stage multiple flux quantum DACs. The last address selects between the COARSE and FINE stages within a DAC. Two such trees were implemented for the 64 DAC circuit reported here.

The first of these is a single flux quantum (SFQ) demultiplexer used as an addressing system. It is constructed as a binary tree of $2^N - 1$ 1:2 SFQ demultiplexer gates as shown in Fig. 1. For the specific design discussed here, the number of address lines N is 6. As discussed below, this demultiplexer allows many devices to be addressed using only a few address lines.

The second part is a set of digital to analog converters (DACs), located at the leaves of the address tree. These DACs comprise storage inductors that can hold an integer number of single magnetic flux quanta ($\Phi_0 = h/2e$). Their digital input are single flux quanta, and their analog output are the stored flux which can be coupled into a target device. The magnitude of this output flux is proportional to the number of stored flux quanta. Each DAC has two such storage inductors, a COARSE stage, and a FINE stage, named for the relative strength with which their output flux is coupled to the target device. In our architecture, the output of these DACs is static.

The third part is a method for converting the static output of a DAC to a time-dependent signal. This is achieved by coupling the output of the DAC into a variable gain element, equivalent to the tunable coupler described elsewhere [4]. An analog line carrying a time-dependent current is coupled to the target device via the variable gain element. This approach is useful in the types of circuits of interest here because single

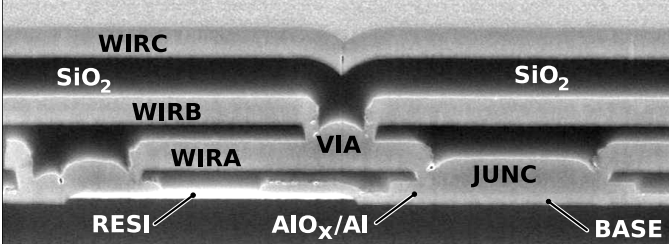


Fig. 2. FIB cut SEM cross-section for the process used to fabricate the circuits described here. The top layer dielectric of this particular sample was not planarized, whereas in the process used to produce the circuits reported upon, all dielectric layers were planarized.

analog lines can be shared among large numbers of devices that need the same functional dependence on time, but may require individual tunability of the gain and offset.

We designed, fabricated and operated an integrated circuit comprising this type of control system architecture. The circuit includes eight superconducting rf-SQUID flux qubits as described by Reference [5], each of which has inductive ports coupled to five different DACs, and 24 compound Josephson junction (CJJ) rf-SQUID couplers [4], each of which is coupled to a single DAC. Thus, this circuit required $8 \times 5 + 24 = 64$ DACs. The particular control circuit described here comprises two 1:32 demultiplexers with six shared address lines and two separate power lines. This circuit included 1,538 junctions ranging in size from a minimum of $0.6 \mu\text{m}$ diameter (32 of them) to a maximum of $4 \mu\text{m}$ in diameter.

The paper is organized as follows: Requirements on control circuitry derived from the devices, architecture and operating procedures in superconducting adiabatic quantum optimization systems are discussed in section II. The specific control circuitry architecture is discussed in section III. Data demonstrating the performance relative to requirements is presented in section IV. Conclusions are presented in section V.

The measurements reported in section IV were performed on two different chips fabricated in a four Nb layer superconducting process employing a standard Nb/AIOx/Nb trilayer, a TiPt resistor layer, and planarized PECVD SiO₂ dielectric layers. Design rules included $0.25 \mu\text{m}$ lines and spaces for wiring layers and a minimum junction diameter of $0.6 \mu\text{m}$. A sample process cross section, with all but the top dielectric planarized, is shown in Fig. 2.

II. CONTROL CIRCUITRY REQUIREMENTS

Our intent is to embody a specific quantum algorithm in hardware. This algorithm, known as adiabatic quantum optimization (AQO), is a novel approach for solving combinatorial optimization problems. Unlike the incumbent techniques for such problems, such as simulated annealing or genetic algorithms, AQO algorithms include procedures that are explicitly quantum mechanical. The requirement to provide the quantum mechanical resources necessary for running this algorithm places unusual constraints on processor systems and components.

Algorithm 1: The AQO algorithm.

Data: A run-time t_f ; an allowed edge set E ; an N dimensional vector \vec{h} and an upper diagonal $N \times N$ matrix \hat{K} with $h_j, K_{ij} \in \mathcal{R}$ and $K_{ij} \in E$.
Result: A set $\{s_j^*\}$, $s_j \in \{-1, +1\}$, that minimizes

$$\mathcal{E}(s_1, \dots, s_N) = \sum_{j=1}^N h_j s_j + \sum_{i,j \in E} K_{ij} s_i s_j.$$

- 1 Set $t_f = 1 \mu\text{s}$;
- 2 Load \vec{h} and \hat{K} values into hardware;
- 3 Wait 1 ms for hardware to cool down;
- 4 **while** *solution not satisfactory* **do**
- 5 **Run annealing algorithm;**
- 6 Read out qubits to generate trial solution $\{s_j^*\}$;
- 7 **if** $\{s_j^*\}$ *satisfactory* **then**
- 8 | exit;
- 9 **else**
- 10 | $t_f \rightarrow 2t_f$;
- 11 **end**
- 12 **end**

Algorithm 2: The annealing algorithm.

Data: A run-time t_f ; a set of qubits with Hamiltonian

$$H(s) = A(s)H_I + B(s)H_F, \text{ where } s = t/t_f,$$

$$0 \leq s \leq 1, H_I = \sum_{j=1}^N \sigma_{x,j},$$

$$H_F = \sum_{j=1}^N h_j \sigma_{z,j} + \sum_{i,j \in E} K_{ij} \sigma_{z,i} \sigma_{z,j},$$

where $\sigma_{x,j}$ and $\sigma_{z,j}$ are the Pauli σ_x and σ_z matrices for qubit j respectively, and $A(s)$ and $B(s)$ are envelope functions with units of energy such that $A(0)/B(0) \gg 1$ and $A(1)/B(1) \ll 1$.
Result: Evolution of $H(s)$ from $H(0)$ to $H(1)$.

- 1 Set $s = 0$;
- 2 Wait 1 ms for hardware to reach ground state of $H(0)$;
- 3 Ramp currents on global analog lines to drive evolution $s \rightarrow 1$

Quantum computation intimately ties the physics of the underlying hardware to its intended algorithmic use. Primarily motivated by this observation, the approach we have taken to design hardware is a top-down one. For the circuits considered here, the requirements are driven by what is required to run the AQO algorithm. To provide context for the material in this section we first provide an overview of the algorithm itself.

Consider the following discrete optimization problem: Given a vector \vec{h} and upper diagonal matrix \hat{K} , where the elements of both are real numbers, find the set $\{s_i^*\}$ that minimizes the objective function

$$\mathcal{E}(s_1, \dots, s_N) = \sum_{j=1}^N h_j s_j + \sum_{i,j \in E} K_{ij} s_i s_j \quad (1)$$

where $s_i \in \{-1, +1\}$, and E is an set of (i, j) pairs where K_{ij} is allowed to be non-zero. We call E the *allowed edge set*. The necessity for explicitly defining the set E arises because ultimately we will connect this term in the objective function to physical couplings between pairs of qubits, and for a variety of reasons the number of elements in E will generally be much

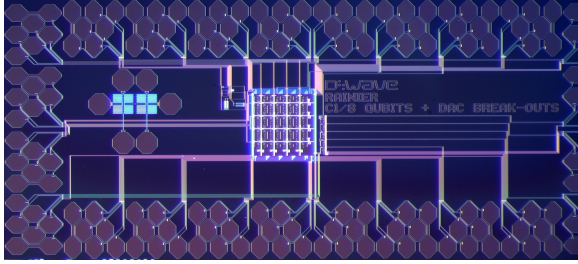
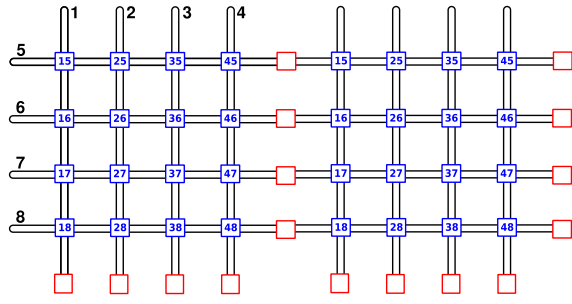


Fig. 3. **Top:** Schematic showing two eight-qubit unit cells tiled together. The qubits are schematically shown as the extended black loops, similar to the way these devices are physically implemented. The couplers (shown as blue and red squares) are local to the intersections of qubits. **Bottom:** Photograph of a standalone eight qubit unit cell occupying a $700\mu\text{m} \times 700\mu\text{m}$ square on a $3\text{ mm} \times 7\text{ mm}$ chip.

less than the total number of possible pairs $N(N-1)/2$. A design constraint on processor architecture is that qubits must be connected in such a way so that finding the minimum of Eq. (1) is NP-hard. Even with this constraint, it is straightforward to find realizable sets E for which this holds, and we will focus exclusively on these cases.

An AQO algorithm exists for solving this problem. The approach is outlined in Algs. 1 and 2. The control system reported on here enters into these in step 2 of Alg. 1. Step 6 of Alg. 1 is performed by a readout system reported on by Berkley *et al.* [6].

A. Processor Interconnect Architecture

There are many possibilities for how one might try to build a hardware system capable of running Algs. 1 and 2. Here we focus on a unit cell consisting of eight qubits and 24 couplers. See Fig. 3 for a schematic and optical photograph showing the interconnect pattern. Larger systems are designed by tiling the plane with increasing numbers of unit cells, as indicated in the top of Fig. 3. This choice of unit cell fixes the allowed edge set E , and satisfies the constraint that minimizing Eq. 1 be NP-hard.

B. Number of DACs

The total number of DACs required for circuits of increasing complexity is shown in Table I. Here we provide a brief overview of how these numbers arise, and refer the reader to [4], [5] for further details.

1) *One DAC per Coupler:* A tunable compound Josephson junction rf-SQUID coupler inductively coupled to qubits i and j is used to set each desired value of K_{ij} [4]. One such physical

TABLE I
PARTS COUNT VS. NUMBER OF UNIT CELLS.

Unit Cells	Qubits	Couplers	DACS	JJs
1	8	16	56	1500
4	32	72	232	6000
16	128	328	968	24000
64	512	1416	3976	96000
256	2048	5896	16136	384000

device is required per element of the allowed edge set E . Couplers are controlled using a static dc flux bias applied to their compound junction—no time dependence in this signal is required. For this design, the flux bias is provided by the DAC shown in red in Fig. 4.

2) *Five DACs per Qubit:* The potential energy of an ideal compound Josephson junction rf-SQUID qubit is [7]

$$\mathcal{U} = -\frac{\Phi_o \mathcal{I}_c}{2\pi} \cos\left(\frac{2\pi\Phi_q}{\Phi_o}\right) \cos\left(\frac{\pi\Phi_{\text{CJJ}}}{\Phi_o}\right) + \frac{(\Phi_q - \Phi_q^x)^2}{2L_q} + \frac{(\Phi_{\text{CJJ}} - \Phi_{\text{CJJ}}^x)^2}{2L_{\text{cjj}}} \quad (2)$$

where \mathcal{I}_c is the *sum* of Josephson critical currents in the compound junction, L_q and L_{cjj} are the inductance in the qubit and compound junction loop, respectively. Likewise Φ_q , Φ_q^x , and Φ_{CJJ} , Φ_{CJJ}^x are the internal and applied flux for the qubit and CJJ loop respectively.

Eq. 2 is only applicable when the two junctions making up the compound junction are identical. Junction critical current \mathcal{I}_c s of identically drawn Josephson junctions in superconductor fabrication processes are reported to have a normal distribution with a standard deviation of anywhere from 1% to 5% [8]. Thus, we expect real compound junctions to be naturally imbalanced. This causes difficulties in running the annealing algorithm Alg. 2 [5]. To overcome this junction imbalance problem we use a more complex structure which we call a compound compound Josephson junction (CCJJ). This provides two additional degrees of control freedom per qubit, which can be used to correct for reasonable junction imbalance ($\sim 5\%$ \mathcal{I}_c difference). We access these structures via the blue CCJJ minor DACs in Fig. 4.

As inter-qubit coupling strength is adjusted, the susceptibility of the coupler, and the extent to which it inductively loads the qubit, will change [4]. This causes the qubit inductance L_q in Eq. 2 to be dependent upon the choice of $\{K_{ij}\}$. To overcome the resulting problem-dependent inter-qubit imbalance, we add an additional compound junction, comprising much larger junctions, in series with the qubit inductance. We call this structure an L -tuner [5]. The Josephson inductance of this compound junction is modified with application of a flux bias applied through an on-chip flux DAC, shown in green in Fig. 4.

As discussed in Reference [9], care must be taken during annealing to ensure that the final Hamiltonian H_F , the one encoding the problem we wish to solve, is that which was intended. Using a compound junction to modify the relative weights of H_I and H_F causes \tilde{h} and \tilde{K} to change during the annealing algorithm, both in an absolute sense, and relative to each other. This arises because although energy scales \tilde{h} and \tilde{K}

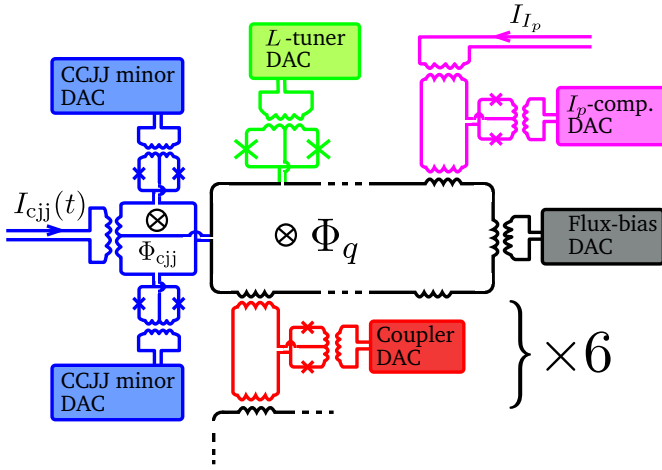


Fig. 4. Single qubit schematic. The five main parts of this qubit design: the qubit main loop (black) with flux-bias DAC providing the flux-bias Φ_q , the CCJJ (blue) with cjj-bias Φ_{cjj} in the major lobe and two DACs biasing the minor lobes, the L-Tuner (green) with DAC, and I_p -compensator (pink) with DAC. Also shown is a coupler (red) with coupler DAC. The two global time dependent control lines (I_{cjj} and I_p) used for running the annealing algorithm are also shown.

are both functions of the persistent currents in the qubits (I_p), they have different functional dependencies. Qubit I_p changes during annealing, distorting H_F .

To keep the relative scale constant, the value of the applied flux used to implement \tilde{h} must change during the annealing, but $\Phi_q(t)$ will be different for each qubit, depending on the intended value of \tilde{h} for that problem. This is accomplished by giving each qubit another tunable coupler, coupled to both the qubit and a shared external analog flux bias line. We call this an I_p -compensator. Each such coupler is used as a variable gain element, programmed with its own DAC (the pink DAC in Fig. 4), and used to scale a global controlled signal to the locally required h_j .

Finally, each qubit has a DAC that can apply a small dc flux bias to its main loop (the black DAC in Fig. 4).

C. Precision and Range Requirements

Requirements on precision and range of flux from the DACs ultimately depend on the precision to which the elements of \tilde{h} and \tilde{K} are to be specified. The system described here was designed to be able to attain four effective bits of precision on parameters h_j and K_{ij} ; in other words, the elements h_j and K_{ij} can be selected from 16 different allowed values. This does not mean that the DACs need only four bits of precision. The DAC requirements are derived from those on Hamiltonian parameters \tilde{h} and \tilde{K} , based on what aspect of a qubit or coupler is being controlled. In our case, requiring four bits of precision in \tilde{h} and \tilde{K} typically translates into a requirement of about eight bits of precision in each of the DACs.

The primary design parameters for each DAC is its dynamic range: how much flux is it necessary for the DAC to provide, and how fine a control of that flux is needed. All of the DACs were designed to cover their respective ranges in subdivisions of either 300 or 400 steps. However, they differ in the total

amount of flux coupled at maximum range from around $25 m\Phi_0$ for the qubit flux bias DAC to as much as $0.9 \Phi_0$ from the coupler DAC. A summary of desired flux ranges and minimal flux steps is shown in Table II.

TABLE II
DESIGNED FLUX RANGES AND MINIMAL FLUX STEPS BY DAC TYPE

DAC Type	Span	min $\Delta\Phi$	Max # Φ_0		COARSE/FINE Ratio
			COARSE	FINE	
Qubit Flux	$25.5 m\Phi_0$	$0.1 m\Phi_0$	17	17	14.1
CJJ Balance	$66.1 m\Phi_0$	$0.4 m\Phi_0$	17	17	14.1
L-Tuner	$0.465 \Phi_0$	$1.1 m\Phi_0$	40	10	10.7
Coupler	$0.968 \Phi_0$	$2.2 m\Phi_0$	40	10	10.6

D. Programming Constraints

In the design discussed here, there are five DACs per qubit and one per coupler that need to be programmed to implement a specific problem instance. While the DACs are being programmed, power is applied to the SFQ circuits in the address tree, and the chip will heat. The amount of time we must wait for it to cool afterwards (step 3 in Alg. 1) depends on the peak temperatures reached by the various portions of the circuitry, and the relaxation mechanisms enabling their return to equilibrium [10]. Minimizing overall programming time, including that required to cool, is an important design constraint, and must be considered when comparing control circuitry architectures.

Given the block architecture described above, the number of DACs we must program increases with processor size as shown in Table I. While not every DAC will need to be programmed for each unique configuration of h_j and K_{ij} in practice, in what follows the assumption will be that all are. In our multiple flux quantum based encoding scheme, the programming time will depend on the value programmed. To estimate the basic scaling with number of devices, it is probably reasonable to assume that each time the processor is programmed for a new problem, each DAC stage must receive on average half of its designed capacity in pulses. For example, the coupler DAC would receive about $20(\text{COARSE}) + 5(\text{FINE}) = 25\Phi_0$, the qubit flux bias DAC about $9(\text{COARSE}) + 9(\text{FINE}) = 18\Phi_0$, or roughly $20 \Phi_0$ per DAC in either case.

Programming speed can then be bought at the expense of additional input lines and more parallelization - using more, shallower address trees each with its own separate input.

However, with or without parallelization, one must be able to load all the pulses without errors. The more DACs being programmed, the more pulses there are that must be routed through the address tree with fidelity, and the smaller the acceptable error probability per pulse. For example, per Table I, with 2048 qubits, we require 16,136 DACs. An average problem would require loading $\sim 3.2 \times 10^5$ flux quanta onto the chip. If we want 95% confidence that we can program problems correctly 99 times out of 100, the probability that any flux quanta makes an error should not be greater than 10^{-9} . With 128 qubits, 10^{-8} is sufficient.

Bit error probability in SFQ circuits has been extensively studied [11]. Satisfying these and even more demanding error

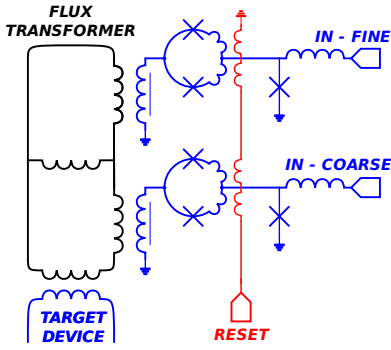


Fig. 5. A two stage DAC made of a pair of separately addressable storage inductors (distinguished by an extra line under the inductor schematic symbol). The flux from each inductor is scaled and summed in a flux transformer into the target output.

rate requirements at sub-Kelvin temperatures is straightforward, but needs to be confirmed for any particular implementation.

III. CONTROL CIRCUITRY ARCHITECTURE

A. Two Stage Multiple Flux Quantum DAC with Reset

The design of the resettable DAC stage is discussed in more detail in Reference [12]. The DACs were made of two stages. Each stage comprises a large storage inductor in series with a two-junction reset SQUID, and an input junction, as shown in Fig. 5. Each stage was designed with $\beta \equiv 2\pi LI_c/\Phi_0$ in the range 75 to 300, depending on their function, and thus able to hold in the range of 10 to 40 flux quanta of either polarity. Here L is the stage inductance, and I_c is the effective critical current of the two junction reset SQUID.

The two-junction reset SQUID is used to empty the DAC stage of stored flux. This is accomplished by applying $\Phi_0/2$ flux to the reset loop, so that its effective critical current $2I_c^{reset} \cos(\pi\Phi_x/\Phi_0)$, and thus DAC stage β , is diminished to below the level required to store flux. For this reset function to be effective, it must be possible to suppress the effective critical current of the reset SQUID to less than that required to store one Φ_0 in the storage inductor. This requirement places an upper bound on the DAC stage β . It also places a requirement on how closely matched the I_c s of the two junctions in the reset SQUID must be to each other. This is because the minimum effective critical current will not be less than the difference in the I_c s of the two reset junctions. Thus given a particular fabrication process, with its feature size, penetration depths, and characteristic junction I_c spread, there will be some maximum number of Φ_0 that can be stored in a DAC that can be reliably reset to an empty state. This limits the dynamic range of an individual DAC stage.

We can achieve a dynamic range greater than that of an individual DAC stage, and shorten programming times, by connecting two or more stages together, as indicated in Fig. 5. The intervening transformer couples the different stages into the target circuit with different weights. The flux transformer can be thought of as playing the role of an R-2R ladder, such as is frequently used in construction of semiconductor DACs. One important difference is that successive stages of this DAC

differ from each other not by factors of two, but more typically by a factor of ten, depending on the requirements set by the target device. The other difference is that we are transforming and dividing flux rather than voltage.

The flux coupled out of this DAC can be summarized by the expression:

$$\Phi_{OUT} = k \cdot \left(N_{COARSE} \Phi_0 + \frac{1}{\gamma} \cdot N_{FINE} \Phi_0 \right) \quad (3)$$

where $N_{COARSE, FINE}$ represent the integer number of flux quanta that are stored within the respective DAC stages, k the coupling constant describing the amount of flux from the COARSE stage into the output device, and γ , the division ratio between COARSE and FINE, which is typically 10 for the devices discussed here.

B. Programmable time-dependent signals

As discussed in section II-B.2, we require the ability to supply time dependent signals to each of the qubits to compensate for the fact that the qubit persistent current changes during the annealing process. These time dependent signals need to have the same temporal shape but with different magnitudes. The DACs discussed above can hold static flux, and are not suited to provide real-time signals. This is because they do not include a sample-and-hold stage to protect the output from transients during programming. Moreover, real-time updating of the DACs would raise the temperature of the chip to an unacceptable level.

Rather, time dependent signals can be customized using the tunable coupler discussed in Reference [4] as a variable or programmable gain element. A global analog bias line holding a *master copy* of the desired time dependent signal is coupled to each qubit on the chip through its own programmable gain element, as indicated in Fig. 6. Each programmable gain element is controlled by its own DAC. In conjunction with an additional DAC (not shown) to provide a flux offset to each target device, the *master copy* of the signal can be uniquely transformed for each target in the following manner:

$$\Phi_i(t) = a_i + g_i \Phi_{global}(t) \quad (4)$$

where a_i and g_i are programmable on a per device basis. This is not as flexible as having independent arbitrary waveform generators for each device, but it is flexible enough to satisfy the requirements of the I_P compensator.

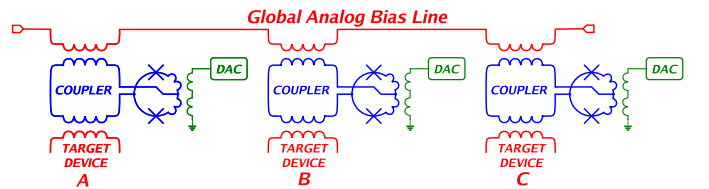


Fig. 6. A time dependent current on a global analog bias line can be uniquely scaled into each of several target devices by using independent programmable gain elements (blue), each controlled with its own DAC (green).

and COARSE weights (k and γ) can be extracted. Data from parameters extracted in this way is presented in Table III. Second, within the body of the circuit block, wherever a DAC is used to apply a flux bias, an analog line is also used to flux bias that target device in parallel with that DAC. This combination is indicated in the inset of Fig. 9. This single analog line is shared amongst all like control nodes for all qubits, so that only a handful of such lines are required to service the entire chip. Of course, the shared analog line cannot be used for independent control of all devices simultaneously, but it is nevertheless useful for testing individual devices. For example, each qubit is flux biased by its own DAC *and* a single shared externally accessible analog line. The qubit degeneracy point is easily measured [6]. If the DAC is then programmed with, for example, $+5\Phi_0$ in its COARSE stage, one can determine the change in current on that analog qubit flux bias line required to compensate for the shift in degeneracy point. This allows us to find the ratio of mutual inductance between the analog line and the qubit to that between each DAC stage (COARSE & FINE) and the qubit. We can independently measure the mutual inductance of the analog line into the qubit by noting the Φ_0 periodicity in its response. We can then determine k and γ for that DAC, which are the parameters we need to determine how much flux the DAC applies to its target.

This feedback measurement is applicable to determining k and γ for DACs used for various types of control, not just qubit flux bias. The only thing that differs is the nature of the measured quantity. For the qubit flux bias DAC, the qubit degeneracy point was mentioned. For the L-Tuner DAC, a measure of the qubit's inductance, ultimately a measure of its circulating current, can be used. For the CCJJ DACs, a measure that quantifies the imbalance in the qubit's compound junction is used. In all cases we use the measured quantity to determine what analog signal is necessary to compensate for a change in the programmed DAC state. In this way we can determine how much flux each DAC on chip applies to its target.

A. DAC Biasing a DC SQUID

The couplers shown in red in Fig. 3 are designed to couple qubits between different unit cells. For the eight qubit unit cell under study here these were not connected to qubits on both ends. Instead, the inter-unit cell couplers were wired up in such a way that their compound junction, still biased by its own DAC, could be operated as a hysteretic dc-SQUID. This coupler's DAC could thus be used to apply flux to a dc-SQUID, and so we traced out the I_c vs Φ threshold characteristics for this dc-SQUID as discussed in Reference [6]. The I_c vs Φ curve shown in Fig. 9 was taken both with an analog flux bias controlled directly from room temperature electronics ((a), blue dots) or using the DAC ((a), black circles). To make such a plot, we have to know the coupling constant k between the COARSE DAC stage and the dc-SQUID it biases, as well as the mutual inductance between the analog bias line and the dc-SQUID. As mentioned earlier, the mutual inductance between analog line and dc-SQUID is easily determined by observing the periodicity of the modulation curve. Also discussed earlier,

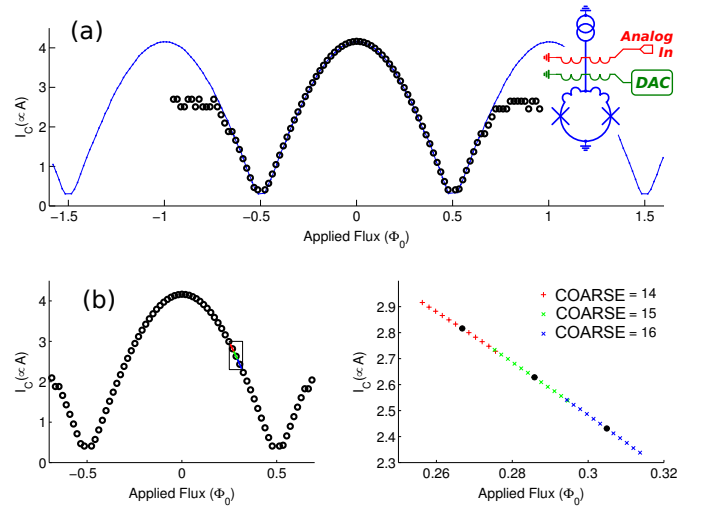


Fig. 9. (a) I_c vs. applied flux modulation curve of a small β two junction hysteretic SQUID where flux was applied with (blue dots) external analog bias current and (black circles) a two-stage superconducting DAC with greater than Φ_0 total span. The black circles are plotted for integer units of Φ_0 sent to the COARSE DAC stage. (b) SQUID modulation curve with integral COARSE values along with that taken exercising the FINE DAC stage around COARSE = 14 (red), 15 (green), and 16 (blue). (c) Expansion of boxed region in (b). Schematic shown in inset.

the coupling constant k and division ratio γ are measured separately with a feedback procedure.

The two threshold curves shown in Fig. 9a begin to deviate from each other past about $\pm 0.65\Phi_0$. This corresponds to where the COARSE stage of this DAC has reached its capacity, and fails to store additional flux. To be clear, the black circles are plotted vs. *flux programmed into* the DAC COARSE stage, not flux actually applied by that DAC stage to the dc-SQUID. A plot of the latter would fall on top of the blue dots.

Fig. 9b shows the same threshold curve vs. flux programmed into the COARSE stage (black dots), but in addition, at COARSE values of $+14\Phi_0$, $+15\Phi_0$, and $+16\Phi_0$, flux ranging from $-\Phi_0$ to $+\Phi_0$ is programmed into the FINE DAC stage as well. This is shown in the boxed region in Fig. 9b, which in turn is expanded in Fig. 9c. In Fig. 9c, it is clear that there is sufficient range in the FINE DAC stage to bridge the COARSE DAC steps.

To use the DAC, it is necessary for the reset function to operate. A reset pulse, made by first increasing the flux bias on the reset dc-SQUID shown in Fig. 5 from zero to beyond $\Phi_0/2$, and then reducing it back to zero, was usually adequate to reset the DAC. There were cases when the I_c s of reset junctions for a particular DAC stage differed from each other by more than about 5%, where a single pulse was not sufficient, and the DAC would occasionally retain one or two Φ_0 . In these cases, the reset pulse had to be repeated several times to consistently empty the DAC. While the correlation between junction spread, DAC stage β , and reset function is not quantitatively understood by us, we expect the problem to worsen with increased junction I_c spread, and with increased DAC stage storage capacity (β). We found that for the chips reported upon here, it was always possible to reset all of the DAC stages.

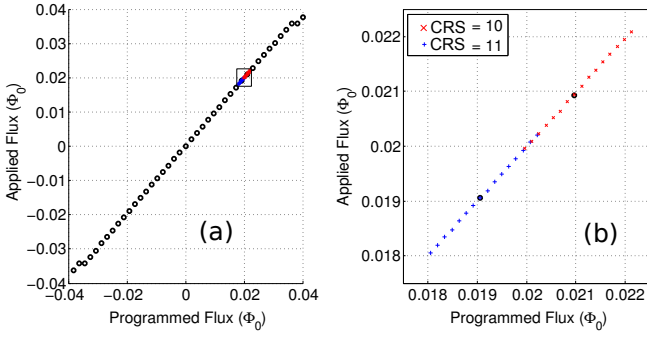


Fig. 10. (a) Flux response vs. flux programmed into the COARSE (black circles) qubit flux DAC. (b) Expanded scale of the boxed region in (a) shows response of the FINE DAC stage to flux exercised around COARSE = $10\Phi_0$ (blue +) and $11\Phi_0$ (red x). Measurement uncertainty in flux is smaller than the plot symbols.

B. DAC applying flux bias to a qubit

Each qubit has a DAC that can apply a flux bias to its body. Fig. 10 shows the flux response relative to the COARSE and FINE for one of these DACs. The limits of the COARSE stage capacity are just visible at the extrema of the plot. To adequately cover the range, the maximum span achievable with the FINE stage must be enough to cover one step of the COARSE stage. This coverage is clearly attained in Fig. 10.

C. DAC control of inter-qubit coupling

One of the most challenging cases to treat in the design of these DACs was the situation in which a large flux span was to be applied to a low inductance SQUID. This situation is most extreme in the case of the coupler DAC and the L -tuner DAC. In fact, the dc-SQUID threshold curve presented in Fig. 9 above is an example of such a case - these dc-SQUIDs are patterned identically to the compound junction used in the coupler and I_p -compensator.

We can also observe a DAC controlling inter-qubit coupling. Fig. 11 shows a plot of the effective coupling between two qubits, via a tunable coupler, as a function of flux applied to control the coupler by an analog control line (red points). Inter-qubit coupling using the DAC to control the same coupler is shown as blue circles in the same plot. More details about the type of measurement used to obtain this plot are discussed in [4].

While presented as an inter-qubit coupler, a similar device is employed in customizing shared time-dependent signals, as discussed in section III-B. The key difference is that in Fig. 6, one of the qubit ports on the coupler is connected to a global analog bias line. We found it straight forward employing this programmable coupler in the fashion described in section III-B.

D. Summary of DAC performance

Table III(a) summarizes design targets vs. achieved COARSE and FINE step sizes for the various types of DAC implemented on the eight-qubit block. Data from Table III(a) are extracted from separate *break-out* versions of the circuit.

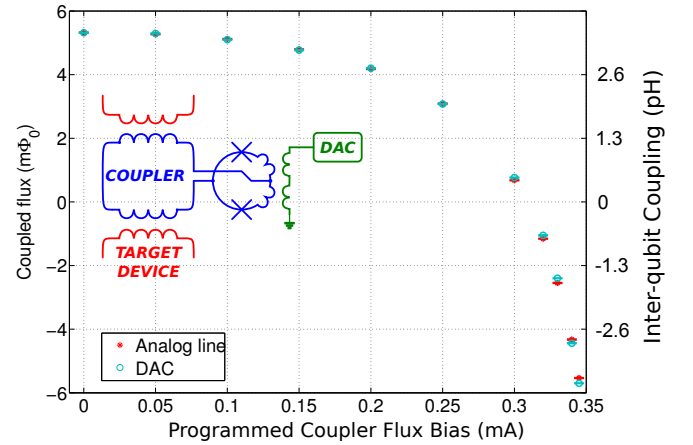


Fig. 11. Effective mutual inductance of an inter-qubit coupler as a function of flux applied by an analog control line (red). The same vs. flux applied by the coupler DAC are shown in blue. Error bars on the plot are smaller than the symbols.

Uncertainties reported derive from the measurement uncertainty of that parameter for that individual device. Measuring these parameters *in-situ* using the feedback technique described above shows device-to-device variation with a standard deviation of around 2%. For example, the distribution of k values measured for the 16 CCJJ DACs on one chip, shown in Fig. 12, exhibits a relative standard deviation of 1.4%. This is consistent with observed variation in mutual inductance of simple microstrip transformers used in this circuit, such as might occur with variations in dielectric thickness of the same scale. Table III(b) summarizes the maximum number of SFQ and maximum coupled flux by each DAC type.

It is worth observing that we were able to confirm that *all* of the two stage DACs on the chips discussed here yielded. By yielded we mean that they behaved as expected, per Tables IIIa and IIIb, and that variations in coupling between identically designed DACs were of the order of 2%. Moreover, there were no significant differences in maximum storage capacity between identically designed copies. This strongly suggests that the DAC storage coils yielded. An inter- or intra-layer short in one of the coils would have compromised the performance of that copy.

Deviations between design targets and achieved parameters for this chip are as large as 30% for some of the couplings. This is primarily due to the challenge of performing sufficiently accurate 3D electromagnetic modeling of the superconducting inductors and transformers used in creating the two-stage DACs.

E. Demonstration of Demultiplexer Functionality

Delivering pulses to the DAC requires that power current and address signals be applied to the demultiplexer tree. Power is shared for all demultiplexer circuits in a particular tree, and address is common for all demultiplexers at a particular level in the tree. The design and fabrication of the chip must be sufficiently uniform such that all cells work with common levels. It is also necessary that the operating margins are wide

TABLE III
DESIGNED VS. ACHIEVED DAC PARAMETERS

DAC Type	COARSE Step ($m\Phi_0$)		FINE Step ($m\Phi_0$)	
	Design	Achieved	Design	Achieved
Qubit Flux	3.0	3.506(3)	0.21	0.268(3)
CCJJ	5.6	3.899(2)	0.40	0.296(3)
L-Tuner	11.3	8.481(1)	1.1	1.061(1)
Coupler	23.6	19.0221(2)	2.2	1.788(1)

(a) COARSE and FINE DAC step weights

DAC Type	MAX COARSE Φ_0		Max Coupled Flux (Φ_0)	
	Designed	Achieved	Designed	Achieved
Qubit Flux	17	22	0.050	0.077
CCJJ	17	22	0.093	0.086
L-Tuner	41	40	0.460	0.339
Coupler	41	35	0.960	0.665

(b) Maximum storage capacity, maximum applied flux

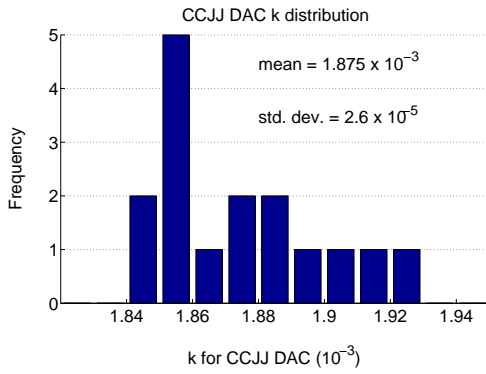


Fig. 12. Distribution of DAC k values for 16 identically designed CCJJ DACs on one of the chips tested. The relative standard deviation is 1.4%.

enough that a robust, low error rate operating point can be obtained.

On this chip there were several DACs attached to unused boundary couplers wired up as dc-SQUIDS. Operating margins required to address the FINE and COARSE DAC stages of each of these were obtained with respect to global power and level of address signal. These operating regions are shown in Fig. 13. Routing an SFQ pulse to a particular DAC requires the successful navigation of six demultiplexer gates, each with its own address current. While the signs of these various address levels may differ, their magnitude in flux was held to a common value, and this common magnitude of address flux is the address axis in Fig. 13.

As far as addressing these six DACs, there is clearly adequate uniformity in this demultiplexer tree that they can all be operated at a common power and address level. We have determined that all 64 DACs on the chip discussed here, as well as those on another subsequently tested, were addressable with chip-wide common power and address levels.

Fig. 13 shows the boundary outside of which the probability of failing to increment a DAC stage is of order 0.1 or higher. As mentioned in section II, we require the error rate to be considerably less than this. The dependence of error

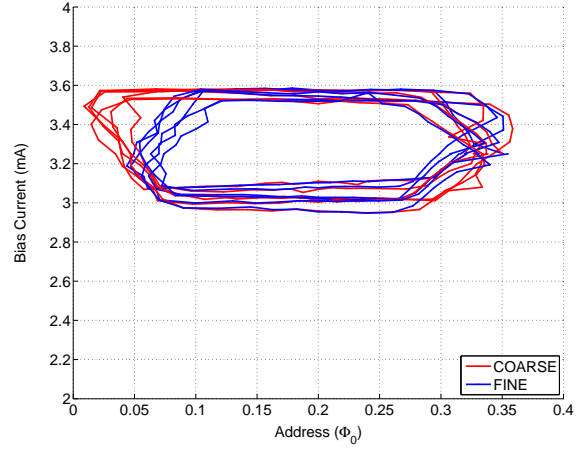


Fig. 13. Combined operating margins in global power current (for one address tree) vs. the magnitude of common address level for six coupler DACs from the same eight qubit circuit block. Two of these are addressed by one of the address trees on the chip, the rest by the other.

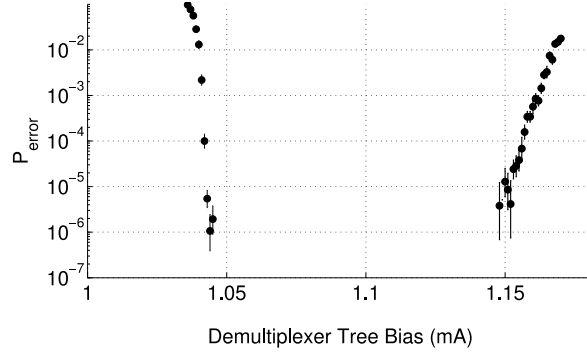


Fig. 14. Dependence of demultiplexer error rate on power current near nominal address levels. At the operating point, P_{error} was bounded to be less than 2.5×10^{-7} with 95% confidence.

probability in SFQ circuits has been studied in some detail by a few different groups [11]. However, we are interested in the aggregate error probability of the entire demultiplexer tree. The probability that a pulse fails to be loaded into a DAC was measured as a function of demultiplexer power at nominal address level, and is shown in Fig. 14.

As expected, the margins decrease as the error probability requirement decreases. There is a significant power range with $P_{error} < 10^{-6}$. At the chosen operating point, no errors were seen in over 15,000,000 operations, which places an upper bound $P_{error} < 2.5 \times 10^{-7}$ with 95% confidence. Reference [12] reports error probability of less than 10^{-8} for a similar demultiplexer tree.

It is not sufficient that the address tree route pulses to the addressed DAC. Rather, it must do so exclusively, and not route pulses to any other DAC. Confirming that pulses arrived at the intended location, a requirement to attain the data shown above, is not sufficient to demonstrate exclusivity.

Indeed if significantly overpowered, with no address applied, the demultiplexer tree is capable of operating in a *broadcast* mode, where pulses are duplicated rather than

routed at each 1:2 demultiplexer node. While this should not happen under normal circumstances, failure to test for this would be an oversight.

Testing exclusivity was performed for most of the DACs on this chip with the following protocol:

- 1) choose a particular DAC stage (COARSE or FINE of a particular DAC)
- 2) verify that this DAC responds correctly when addressed
- 3) Send pulses to every other DAC stage on that tree, and confirm that the state of the particular DAC is not affected.

This was repeated for many of the DACs on the chip at the nominal power and address levels and address tree exclusivity was confirmed in each case.

V. CONCLUSION

We have presented a description of a functioning system of on-chip programmable control circuitry designed to manipulate the parameters and state of rf-SQUID superconducting qubits for use in implementing AQO algorithms. The system is inherently scalable, and in turn allows specialized AQO hardware to be scaled to very large numbers of devices.

Based on classical manipulation of single quanta of magnetic flux, the system was implemented in a planarized four superconductor metal layer process with $0.6\mu\text{m}$ minimum junction diameter and $0.25\mu\text{m}$ lines and spaces for wiring. The control system was fabricated on-chip, in the same process as the qubits and inter-qubit couplers.

Both the two-stage flux DACs used to manipulate the various controls on the qubits, and the demultiplexer address tree used to address those DACs were shown to work as intended. The address tree is shown to pass SFQ pulses with very low error rate, and to address the DACs exclusively. The two-stage DAC design was shown to be effective at providing a flux bias with a dynamic range in excess of eight bits of precision (at dc). The design targets on several variants of DAC were presented, and while the variations between designed and achieved flux coupled into target sometimes reached 30%, this is close enough to satisfy our current requirements.

While the control system described here was designed to operate an AQO processor, it is probable that the devices described - programmable flux DAC, programmable variable gain element, SFQ demultiplexer tree - can be used to control other types of quantum information processors implemented with superconductors.

REFERENCES

- [1] W.M. Kaminsky, S. Lloyd and T.P. Orlando, [arXiv:quant-ph/0403090v2](https://arxiv.org/abs/quant-ph/0403090v2).
- [2] K. K. Likharev and V. K. Semenov, *IEEE Trans. Appl. Supercond.*, 1, 3, (1991). J.P. Hurrell, D. C. Prodmore Brown, A. Silver, *IEEE Transactions on Electron Devices*, October 1980, 1887-1896.
- [3] L.A. Abelson and G.L. Kerber, "Superconductor integrated circuit fabrication technology," *Proc. IEEE*, vol.92, pp. 1517-1533, Oct. 2004; A Silver, A Kleinsasser, G Kerber, Q Herr, M Dorojevets, P Bunyk and L Abelson, "Development of superconductor electronics technology for high-end computing" *Supercond. Sci. Technol.* 16 1368-1374, 2003; <http://www.hypres.com/pages/foundry/bfoundnio.htm>
- [4] R. Harris, T. Lanting, A. J. Berkley, J. Johansson, M. W. Johnson, P. Bunyk, E. Ladizinsky, N. Ladizinsky, T. Oh, and S. Han, "A Compound Josephson Junction Coupler for Flux Qubits With Minimal Crosstalk" *to be published - Description of Qubit Design*
- [5] A. J. Berkley, M. W. Johnson, P. Bunyk, R. Harris, J. Johansson, T. Lanting, E. Ladizinsky, E. Tolkacheva, M. H. S. Amin, G. Rose, "A scalable readout system for a superconducting adiabatic quantum optimization system", [arXiv:0905.0891v1](https://arxiv.org/abs/0905.0891v1)
- [6] S. Han, J. Lapointe, and J. E. Lukens, "Thermal Activation in a Two-Dimensional Potential", *Phys. Rev. Lett.*, **63**, 1712 (1989).
- [7] L.A. Abelson, K. Daly, N. Martinez, and A.D. Smith, "LTS Josephson junction critical current uniformities for FINE applications," *IEEE Trans. Appl. Supercond.*, Vol. 5, pp. 2727-2730, 1995; Nakada, D.; Berggren, K.K.; Macedo, E.; Liberman, V.; Orlando, T.P., "Improved critical-current-density uniformity by using anodization" /em *IEEE Trans. Appl. Supercond.*, Volume 13, Issue 2, June 2003 Page(s): 111 - 114
- [8] R. Harris, A. J. Berkley, J. Johansson, M. W. Johnson, T. Lanting, P. Bunyk, E. Tolkacheva, E. Ladizinsky, B. Bumble, A. Fung, A. Kaul, A. Kleinsasser, and S. Han; "Implementation of a Quantum Annealing Algorithm Using a Superconducting Circuit", [arXiv:0903.3906v1](https://arxiv.org/abs/0903.3906v1), 23 March 2009
- [9] A. M. Savin, J. P. Pekola, D. V. Averin, V. K. Semenov, "Thermal budget of superconducting digital circuits at sub-kelvin temperatures", *J. Appl. Phys.* 99, 084501 (2006)
- [10] Herr Q. P., Feldman M. J., Error rate of a superconducting circuit *Appl. Phys. Lett.* 69, 694 (1996); Herr Q. P., Johnson M. W., Feldman M. J., "Temperature-dependent bit-error rate of a clocked superconducting digital circuit", *IEEE Trans. Appl. Supercond.* 1999, vol. 9 (3), No. 2, pp. 3594-3597; Satchell, J., "Limitations on HTS single flux quantum logic" *IEEE Trans. Appl. Supercond.* Volume 9, Issue 2, Jun 1999 Page(s):3841 - 3844
- [11] *to be published* - E. M. Chapple, M. W. Johnson, P. Bunyk, E. Tolkacheva, I. Perminov, A. B. Wilson, F. Maibaum, A. K. Fung, B. Bumble, A. Kaul, A. Kleinsasser "Design and test of an asynchronous SFQ demultiplexer for applying on-chip flux signals"